2016-06-15

# Optical closure in marine waters from in situ inherent optical property measurements

Lefering, I



10.1364/OE.24.014036
Optics Express
The Optical Society

# Optical closure in marine waters from *in situ* inherent optical property measurements

**Ina Lefering,[1,*] Fethi Bengil,[2] Charles Trees,[3] Rüdiger Röttgers,[4] David Bowers,[5] Alex Nimmo-Smith,[6] Jill Schwarz,[6] and David McKee[1]**

[1]*Physics Department, University of Strathclyde, Glasgow, Scotland, UK*
[2]*Marine School, Girne American University, Girne-TRNC via Mersin 10, Turkey*
[3]*Centre for Maritime Research and Experimentation, La Spezia, Italy*
[4]*Remote Sensing Department, Helmholtz-Zentrum Geesthacht, Geesthacht, Germany*
[5]*School of Ocean Sciences, Bangor University, Wales, UK*
[6]*School of Marine Science and Engineering, Plymouth University, England, UK*
[*]*katharina.lefering@strath.ac.uk*

**Abstract:** Optical closure using radiative transfer simulations can be used to determine the consistency of *in situ* measurements of inherent optical properties (IOPs) and radiometry. Three scattering corrections are applied to *in situ* absorption and attenuation profile data for a range of coastal and oceanic waters, but are found to have only very limited impact on subsequent closure attempts for these stations. Best-fit regressions on log-transformed measured and modelled downwards irradiance, $E_d$, and upwards radiance, $L_u$, profiles have median slopes between 0.92 – 1.24, revealing a tendency to underestimate $E_d$ and $L_u$ with depth. This is only partly explained by non-inclusion of fluorescence emission from CDOM and chlorophyll in the simulations. There are several stations where multiple volume scattering function related data processing steps perform poorly which suggests the potential existence of unresolved features in the modelling of the angular distribution of scattered photons. General optical closure therefore remains problematic, even though there are many cases in the data set where the match between measured and modelled radiometric data is within 25% RMS%E. These results are significant for applications that rely on optical closure e.g. assimilating ocean colour data into coupled physical-ecosystem models.



**OCIS codes:** (010.1030) Absorption; (010.4450) Oceanic optics; (010.5620) Radiative transfer.

## References and links

1. J. A. Yoder, J. K. Moore, and R. N. Swift, "Putting together the big picture: remote-sensing observations of ocean color," Oceanography **14**(4), 33–40 (2001).
2. C. R. McClain, "A decade of satellite ocean color observations," Annu. Rev. Mar. Sci. **1**(1), 19–42 (2009).
3. M. J. Behrenfeld and P. G. Falkowski, "Photosynthetic rates derived from satellite-based chlorophyll concentrations," Limnol. Oceanogr. **42**(1), 1–20 (1997).
4. K. L. Denman and M. A. Peña, "The response of two coupled one-dimensional mixed layer/planktonic ecosystem models to climate change in the NE subarctic Pacific Ocean," Deep-Sea Res. **49**, 5739–5757 (2002).
5. T. D. Dickey, M. R. Lewis, and G. C. Chang, "Optical oceanography: recent advances and future directions using global remote sensing and *in situ* observations," Rev. Geophys. **44**(1), RG1001 (2006).
6. M. Fujii, E. Boss, and F. Chai, "The value of adding optics to ecosystem models: a case study," Bio. Geo. Sci. **4**(5), 817–835 (2007).
7. D. Stramski, R. A. Reynolds, M. Kahru, and B. G. Mitchell, "Estimation of particulate organic carbon in the ocean from satellite remote sensing," Science **285**(5425), 239–242 (1999).
8. D. A. Siegel, S. Maritorena, N. B. Nelson, D. A. Hansell, and M. Lorenzi-Kayser, "Global distribution and dynamics of colored dissolved and detrital organic materials," J. Geophys. Res. **107**(C12), 3228 (2002).
9. Z. Lee, K. L. Carder, and R. A. Arnone, "Deriving inherent optical properties from water color: a multiband quasi-analytical algorithm for optically deep waters," Appl. Opt. **41**(27), 5755–5772 (2002).
10. C. Neil, A. Cunningham, and D. McKee, "Relationships between suspended mineral concentration and red-waveband reflectance in moderately turbid shelf seas," Remote Sens. Environ. **115**(12), 3719–3730 (2011).
11. C. Mitchell, A. Cunningham, and D. McKee, "Remote sensing of shelf sea optical properties: evaluation of a quasi-analytical approach for the Irish Sea," Remote Sens. Environ. **143**, 142–153 (2014).

#264909 Received 11 May 2016; accepted 28 May 2016; published 15 Jun 2016

12. M. Babin, D. Stramski, G. M. Ferrari, H. Claustre, A. Bricaud, G. Obolensky, and N. Hoepffner, "Variations in the light absorption coefficients of phytoplankton, non-algal particles, and dissolved organic matter in coastal waters around Europe," J. Geophys. Res. **108**(C7), 3211 (2003).
13. C. D. Mobley, *Light and Water: Radiative Transfer in Natural Waters* (Academic Press, 1994).
14. J. R. Morrison, "In situ determination of quantum yield of phytoplankton chlorophyll a fluorescence: A simple algorithm, observations, and a model," Limnol. Oceanogr. **48**(2), 618–631 (2003).
15. A. A. Andrew, R. Del Vecchio, A. Subramaniam, and N. V. Blough, "Chromophoric dissolved organic matter (CDOM) in the equatorial Atlantic Ocean: Optical properties and their relation to CDOM structure and source," Mar. Chem. **148**, 33–43 (2013).
16. S. Pegau, J. R. V. Zaneveld, and J. L. Mueller, "Inherent optical property measurement concepts: physical principles and instruments in inherent optical properties: instruments, characterizations, field measurements and data analysis protocols," in *Ocean Optics Protocols for Satellite Ocean Color Sensor Validation*, Mueller, J. L., G. S. Fargion and C. R. McClain, eds., NASA/TM-2003–211621/Rev4-Vol.IV (2003).
17. D. McKee, J. Piskozub, R. Röttgers, and R. Reynolds, "Evaluation and Improvement of an Iterative Scattering Correction Scheme for *in situ* Absorption and Attenuation Measurements," J. Atmos. Ocean. Technol. **30**(7), 1527–1541 (2013).
18. J. R. V. Zaneveld, J. C. Kitchen, and C. M. Moore, "The scattering error correction of reflecting-tube absorption meters," Proc. SPIE **2258**, 44–55 (1994).
19. M. S. Twardowski, J. M. Sullivan, P. L. Donaghay, and J. R. V. Zaneveld, "Micro-scale quantification of the absorption by dissolved and particulate material in coastal waters with an AC-9," J. Atmos. Ocean. Technol. **16**(6), 691–707 (1999).
20. L. Eisner, M. S. Twardowski, T. J. Cowles, and M. J. Perry, "Resolving phytoplankton photoprotective: photosynthetic carotenoid ratios on fine scales using *in situ* spectral absorption measurements," Limnol. Oceanogr. **48**(2), 632–646 (2003).
21. J. M. Sullivan, M. S. Twardowski, J. R. V. Zaneveld, C. M. Moore, A. H. Barnard, P. L. Donaghay, and B. Rhoades, "Hyperspectral temperature and salt dependencies of absorption by water and heavy water in the 400-750 nm spectral range," Appl. Opt. **45**(21), 5294–5309 (2006).
22. J. Piskozub, D. Stramski, E. Terrill, and W. K. Melville, "Influence of forward and multiple light scatter on the measurement of beam attenuation in highly scattering marine environments," Appl. Opt. **43**(24), 4723–4731 (2004).
23. E. Boss, W. H. Slade, M. Behrenfeld, and G. Dall'Olmo, "Acceptance angle effects on the beam attenuation in the ocean," Opt. Express **17**(3), 1535–1550 (2009).
24. R. Röttgers, W. Schönfeld, P.-R. Kipp, and R. Doerffer, "Practical test of a point-source integrating cavity absorption meter: the performance of different collector assemblies," Appl. Opt. **44**(26), 5549–5560 (2005).
25. R. Röttgers, D. McKee, and S. B. Wozniak, "Evaluation of scatter corrections for AC-9 absorption measurements in coastal waters," Methods Oceanography **7**, 21–39 (2013).
26. L. G. Sokoletsky and F. Shen, ""Optical closure for remote-sensing reflectance based on accurate radiative transfer approximations: the case of Changjiang (Yangtze) River Estuary and its adjacent coastal area," China," Int. J. Remote Sens. **35**(11-12), 4193–4224 (2014).
27. D. Antoine, A. Morel, E. Leymarie, A. Houyou, B. Gentili, S. Victori, J.-P. Buis, N. Buis, S. Meunier, M. Canini, D. Crozel, B. Fougnie, and P. Henry, "Underwater radiance distributions measured with miniaturized multispectral radiance cameras," J. Atmos. Ocean. Technol. **30**(1), 74–95 (2013).
28. K. J. Voss, "Use of the radiance distribution to measure the optical absorption coefficient in the ocean," Limnol. Oceanogr. **34**(8), 1614–1622 (1989).
29. G. C. Chang, T. D. Dickey, C. D. Mobley, E. Boss, and W. S. Pegau, "Toward closure of upwelling radiance in coastal waters," Appl. Opt. **42**(9), 1574–1582 (2003).
30. C. D. Mobley, L. K. Sundman, and E. Boss, "Phase function effects on oceanic light fields," Appl. Opt. **41**(6), 1035–1050 (2002).
31. M. Tzortziou, J. R. Herman, C. L. Gallegos, P. J. Neale, A. Subramaniam, L. W. Harding, Jr., and Z. Ahmad, "Bio-optics of the Chesapeake Bay from measurements and radiative transfer closure," Estuar. Coast. Shelf Sci. **68**(1-2), 348–362 (2006).
32. G. Chang, A. Barnard, and J. R. Zaneveld, "Optical closure in a complex coastal environment: particle effects," Appl. Opt. **46**(31), 7679–7692 (2007).
33. G. Chang and A. L. Whitmire, "Effects of bulk particle characteristics on backscattering and optical closure," Opt. Express **17**(4), 2132–2142 (2009).
34. M. Talaulikar, T. Suresh, E. Desa, and A. Inamdar, "Optical closure of apparent optical properties. coastal waters off goa," J. Ind. Soc. Rem. Sens. **43**(1), 163–171 (2015).
35. B. Bulgarelli, G. Zibordi, and J.-F. Berthon, "Measured and modeled radiometric quantities in coastal waters: toward a closure," Appl. Opt. **42**(27), 5365–5381 (2003).
36. T. J. Petzold, "Volume scattering functions for selected ocean waters," Tech. Rep. SIO **7278** (Scripps Institution of Oceanography, 1972), pp. 72–78.
37. P. D. Biber, C. L. Gallegos, and E. J. Kenworthy, "Calibration of bio-optical model in the North River, North Carolina: A tool to evaluate water quality impacts on seagrasses," Estuaries Coasts **31**, 177–191 (2008).
38. C. L. Gallegos, R. J. Davies-Colley, and M. Gall, "Optical closure in lakes with contrasting extremes of reflectance," Limnol. Oceanogr. **53**(5), 2021–2034 (2008).
39. D. M. O'Donnell, S. W. Effler, C. M. Strait, F. Peng, and M. Perkins, "Remote sensing reflectance in the Great Lakes: *In situ* measurements, closure analyses and a forward model," J. Great Lakes Res. **39**, 137–150 (2013).

#264909 Received 11 May 2016; accepted 28 May 2016; published 15 Jun 2016

40. W. S. Pegau, D. Gray, and J. R. V. Zaneveld, "Absorption and attenuation of visible and near-infrared light in water: dependence on temperature and salinity," Appl. Opt. **36**(24), 6035–6046 (1997).
41. S. Tassan and G. M. Ferrari, "Variability of light absorption by aquatic particles in the near-infrared spectral region," Appl. Opt. **42**(24), 4802–4810 (2003).
42. M. Chami, E. B. Shybanov, T. Y. Churilova, G. A. Khomenko, M. E.-G. Lee, O. V. Martynov, G. A. Berseneva, and G. K. Korotaev, "Optical properties of the particles in the Crimea coastal waters (Black Sea)," J. Geophys. Res. **110**(C11), C11020 (2005).
43. D. McKee and A. Cunningham, "Evidence for wavelength dependence of the scattering phase function and its implication for modeling radiance transfer in shelf seas," Appl. Opt. **44**(1), 126–135 (2005).
44. WET Labs Inc, "Scattering meter, ECO BB-9, User's Guide" Revision L, 9–10 (2013).
45. A. Morel, "Optical properties of pure water and pure seawater," in *Optical Aspects of Oceanography*, N. G. Jerlov and E. S. Nielsen, eds. (Academic, 1974), pp. 1–24.
46. E. Boss and W. S. Pegau, "Relationship of light scattering at an angle in the backward direction to the backscattering coefficient," Appl. Opt. **40**(30), 5503–5507 (2001).
47. J. M. Sullivan, M. S. Twardowski, P. L. Donaghay, and S. A. Freeman, "Use of optical scattering to discriminate particle types in coastal waters," Appl. Opt. **44**(9), 1667–1680 (2005).
48. M. S. Twardowski, H. Claustre, S. A. Freeman, D. Stramski, and Y. Huot, "Optical backscattering properties of the 'clearest natural' waters," Bio. Geo. Sci. **4**, 1041–1058 (2007).
49. K. Voss, H. Gordon, M. Lewis, S. McLean, M. Twardowski, C. Johnson, M. Yarbrough, S. Flora, M. Feinholz, and C. Trees, "Radiometry and uncertainties from SORTIE (Spectral Ocean Radiance Transfer Investigation and Experiment)," in *NASA Carbon Cycle and Ecosystem Joint Science Workshop* (2008).
50. J. L. Mueller, "In-water radiometric profile measurements and data analysis protocol in radiometric measurements and data analysis protocols," in *Ocean Optics Protocols for Satellite Ocean Color Sensor Validation*, Mueller, J. L., G. S. Fargion and C. R. McClain, eds., NASA/TM-2003–211621/Rev4-Vol.III (2003).
51. V. Sanjuan Calzado, D. McKee, and C. Trees, "Multi and single cast radiometric processing and merging in the Ligurian Sea," in *Optics of Natural Waters 2011* (2011).
52. G. R. Fournier and J. L. Forand, "Analytic phase function for ocean water," Proc. SPIE **2258**, 194–201 (1994).
53. H. R. Gordon, "Sensitivity of radiative transfer to small-angle scattering in the ocean: Quantitative assessment," Appl. Opt. **32**(36), 7505–7511 (1993).
54. T. Harmel, M. Hieronymi, W. Slade, R. Röttgers, F. Roullier, and M. Chami, "Laboratory experiments for inter-comparison of three volume scattering meters to measure angular scattering properties of hydrosols," Opt. Express **24**(2), A234–A256 (2016).

## 1. Introduction

Ocean colour remote sensing (OCRS) has transformed our ability to observe complex interactions between physical and biogeochemical processes in surface waters of the ocean [1,2]. It has provided new insights into the spatial and temporal variability of algal blooms, sediment transport and a host of other features that were previously only poorly observed [3,4]. The availability of a continuous time series of global ocean colour data that has increased in duration to climate relevant timescales, together with the development of coupled physical-ecosystem models of ever increasing scope and sophistication, has led to increasing demand to use OCRS data for assimilation into and validation of modelled systems [5]. OCRS products provide physical (e.g. inherent optical properties, sea surface temperature) and biogeochemical (e.g. chlorophyll, total suspended solids) parameters that can be assimilated into and used to validate physical-ecosystem models. However, it has to be realised that this approach is effectively an exercise in optical closure i.e.there is an implicit assumption that retrieved parameters and radiometric data are mutually consistent. This leads to the important question: How close to optical closure can we reasonably expect to get with currently available technology?

This paper attempts to address the question of optical closure from the point of view of a best-case scenario where a full depth profile of inherent optical properties is available for each station and underwater and water-leaving light fields can be simulated using a well-developed radiative transfer (RT) model. The degree of optical closure that can be achieved is then assessed against concurrent *in situ* radiometry profiles. This exercise is relevant for a number of applications. For example, Fujii *et al.* [6] have shown the advantages of integrating optical and radiative transfer models into existing ecosystem models, particularly improving modelled subsurface light fields as the main driver for many photo-chemical processes. Data from radiative transfer models are also commonly used to develop satellite remote sensing algorithms [7–11]. Understanding the practical performance limitations for modelling

#264909 Received 11 May 2016; accepted 28 May 2016; published 15 Jun 2016

underwater light fields is essential in the context of ensuring that radiative transfer models are interpreted appropriately.

The inherent optical properties (IOPs) of natural waters, including light absorption $a(\lambda)$, attenuation $c(\lambda)$ and backscattering coefficients $b_b(\lambda)$, are determined by the properties of seawater itself and of other suspended and / or dissolved materials such as phytoplankton, sediments and coloured dissolved organic materials [12]. RT models using depth profiles of spectrally resolved IOPs as input can be used to simulate underwater and water-leaving light fields. Various boundary conditions such as solar elevation, surface roughness, and cloud cover also influence the resulting light fields. Inelastic scattering processes have a significant impact on RT model outputs [13]. Raman scattering by water is ubiquitous and can usually be easily incorporated into models, but fluorescence by phytoplankton and coloured dissolved organic materials (CDOM) require that distributions of these constituents be specifically identified and characterized (e.g. fluorescence quantum yields), which is not trivial due to variability in chemical composition and fluorescence quantum yields [14,15].

The range of instruments that can provide a comprehensive suite of *in situ* IOP measurements required to fully parameterise a RT simulation is relatively small, and the most common configurations would be a combination of a WETLabs AC-9 or AC-S instrument to measure $a(\lambda)$ and $c(\lambda)$, and either a WETLabs BB-9 or HobiLabs HS-6 instrument to measure $b_b(\lambda)$. In all cases, these instruments produce data that requires subsequent correction for temperature, salinity and either scattering or absorption effects, or both [16]. Moreover instrument calibration is critical, requires regular updating to track inevitable sensor degradation with time and use, and in some cases (e.g. BB-9 calibration with standard beads) is not easily performed during research cruises.

Recent work on IOP measurement uncertainties has focused on scattering errors inherent in the designs of the AC-9/-S absorption and attenuation sensors. The absorption sensor is based on a reflective tube design that attempts to gather scattered photons using total internal reflection at the exterior wall of a glass flow cell. Monte Carlo simulation of this arrangement demonstrates partial collection of scattered light up to the critical angle of ~41° and failure to collect beyond this angle [17]. The resulting loss of scattered photons leads to a systematic overestimation of absorption. Various scattering correction approaches have been suggested that invoke different assumptions about the spectral nature of the scattering and volume scattering coefficients and the absorption coefficient in the near-infrared. Of these, the *proportional* correction [18] for the AC-9 absorption measurement has been most commonly used in the past [11,19–21]. The attenuation sensor uses a traditional lens – aperture arrangement to attempt to only collect light that has been directly transmitted through the sample volume. In this case, the source of error is inadvertent collection of photons that have been scattered in forward directions smaller than the collection angle of the lens-aperture system which is ~0.9° in water for the AC-9/-S [22]. Although this error source has long been understood [16], there has been no consensus within the community on an appropriate scattering correction and $c(\lambda)$ has generally been left uncorrected. Boss *et al.* [23] demonstrated that AC-9/-S attenuation data were systematically lower by almost a factor of two than equivalent attenuation data from a LISST100X (Sequoia Scientific), which has a much smaller collection angle (~0.02° in water).

Two new approaches for correcting AC-9/-S data have recently been published, both of which rely to varying extents on the availability of absorption data from a point-source integrating cavity absorption meter (PSICAM), a bench-top instrument that has been demonstrated to provide accurate $a(\lambda)$ data that is free from scattering error artefacts [24]. Röttgers *et al.* [25] presented a *semi-empirical* correction method which is effectively an updated version of the earlier *proportional* correction. In this case, an empirical relationship between the AC-9/-S measured signal and PSICAM data in the near-infrared (NIR) replaces the assumption of zero NIR absorption, and attenuation data are corrected using the average error value from the Boss *et al.* [23] study, with the final correction algorithm maintaining the same basic form as the *proportional* correction and being similarly easy to implement as it only requires AC-9/-S data for input. In contrast, McKee *et al.* [17] presented an alternative

#264909 Received 11 May 2016; accepted 28 May 2016; published 15 Jun 2016

scattering correction methodology that is based upon Monte Carlo simulation of both the absorption and attenuation optical layouts, and uses an iterative model to correct both the absorption and attenuation data. This *iterative* approach requires backscattering data in addition to AC-9/-S data in order to estimate scattering phase functions in the iterative model. The major limitation of this approach, however, was the observation that changes in the reflectivity of the glass flow cell (i.e. degradation with time / use) in the absorption tube could significantly alter the distribution of scattered photons collected by the sensor and that an additional wall reflectance parameter was required to characterise the performance of individual sensors. This was achieved through comparison with PSICAM data, but the limited availability of PSICAM technology in the broader community means that this approach is not as widely available for use as the others.

In broad terms, the two new scattering error approaches for AC-9/-S data appear to offer improvements in the quality of *in situ* $a(\lambda)$ and $c(\lambda)$ data, primarily for coastal waters where scattering errors and NIR absorption by non-algal materials are most significant. Recent results presented by Sokoletsky *et al.* [26] suggest that different scattering corrections for AC-9 absorption measurements can result in up to a 30% difference in remote sensing reflectance modelled using RT. It is therefore interesting to assess the extent to which these correction approaches might impact on optical closure.

Optical closure, in this context, involves the comparison of simulated light field parameters from RT model outputs with *in situ* radiometry measurements. This can take many forms with different parameters offering varying degrees of critical discrimination. For example, use of apparent optical properties (AOPs) such as remote sensing reflectance, $R_{rs}(\lambda)$, or diffuse attenuation coefficient, $K_d(\lambda)$, provide a moderate test of optical closure as these represent properties which are by definition only partly determined by the light field and have close relationships with IOPs. Likewise, testing performance using profiles of photosynthetically available radiation, *PAR*, whilst useful for many ecosystem modelling applications, is a relatively soft test of optical closure as many spectrally-dependent effects are effectively averaged out. At this point in time, the most stringent, practical test of optical closure is by simultaneous comparison against *in situ* profiles of downwards irradiance, $E_d(\lambda)$, and upwards radiance, $L_u(\lambda)$. Full radiance distribution measurements are not widely available but would offer an even more stringent test [27,28]. It is insufficient to test against $E_d(\lambda)$ alone as in most cases this is pinned to the above surface irradiance, $E_s(\lambda)$, which is a boundary condition of the RT model. The combination of $E_d(\lambda)$ and $L_u(\lambda)$ profiles effectively provides an end-to-end test of all the major components of the RT model, with successful modelling of these parameters ensuring the quality of derived higher level products such as radiance reflectance, $R_L(z,\lambda) = L_u(z,\lambda) / E_d(z,\lambda)$ and other AOPs.

Achievement of robust optical closure using *in situ* IOP and radiometry measurements has proven elusive. Several previous studies have attempted to use the failure to achieve optical closure to identify limitations of *in situ* IOP measurements. For example, Chang *et al.* [29] observed $L_w$ and $R_{rs}$ (percentage differences < 29% except for red wavebands) to be sensitive to scattering corrections for AC-9 absorption measurements, the characterisation of chlorophyll fluorescence in the model and assumptions regarding the volume scattering function (VSF) as factors limiting the degree of closure. Their work also highlighted the accuracy of radiance measurements (~25% suggested for *in situ* determinations) as a major source of uncertainty in optical closure tests. Several studies have since investigated the effect of particle characteristics, such as the slope of the particle size distribution and shape of the VSF, on optical closure [30–34]. Bugarelli *et al.* [35], for example, identified the limitation of using an average Petzold phase function [36] for their case studies and additionally observed high sensitivity of modelled in-water radiometric profiles to variations in the bottom reflectance. Studies of fresh water systems, typically complex Case 2 waters, have shown that the degree of closure in waters with high backscattering coefficients remains limited [37–39]. Most studies test optical closure on AOPs, mainly $R_{rs}$, rather than underwater radiometric measurements. Tzortziou *et al.* [31] additionally, attempted optical closure for $E_d$ and $L_u$ profiles and showed excellent agreement for the surface layer (down to 3 m) with percentage

#264909 Received 11 May 2016; accepted 28 May 2016; published 15 Jun 2016

deviations of <18% for $L_u$ and <9% for $E_d$ across the spectrum just beneath the surface (1 m depth). Their work also highlights the sensitivity of RT models to inelastic effects, in particular chlorophyll fluorescence. This study will examine closure results for a range of coastal and deep oceanic waters, test the impact of various IOP correction schemes and report on both surface reflectance parameters and light field parameters at depth.

## 2. Materials and Methods

### *2.1 Sampling*

Data for this study were collected on two cruises, (1) in the Ligurian Sea (LS) off the northwest coast of Italy in March 2009 on board *NR/V Alliance* and (2) off the West Coast of Scotland (WCS) in June 2012 on board *R/V Prince Madog* (Fig. 1). LS stations ranged from deep, clear oceanic waters (classic Case 1) to shallow, turbid stations including some in the plume of the river Arno. WCS stations covered various water types including moderately turbid coastal waters, reasonably clear, potentially Case 1 waters, and a coccolithophore bloom on the edge of the continental shelf. Chlorophyll a (Chl), Total Suspended Solids (TSS) and CDOM ranges for both cruises are given in Table 1.

**Table 1. Ranges of SPM, Chl concentrations and CDOM absorption at 440 nm for the two data sets (LS and WCS).**

| Constituents | Ligurian Sea 2009 | West Coast Scotland 2012 |
|---|---|---|
| Chl [mg $m^{-3}$] | 0.29 - 3.31 | 0.71 - 2.51 |
| TSS [g $m^{-3}$] | 0.133 - 3.77 | 0.91 - 4.02 |
| $a_{CDOM}$(440nm) [$m^{-1}$] | 0.012 - 0.19 | 0.08 – 0.22 |

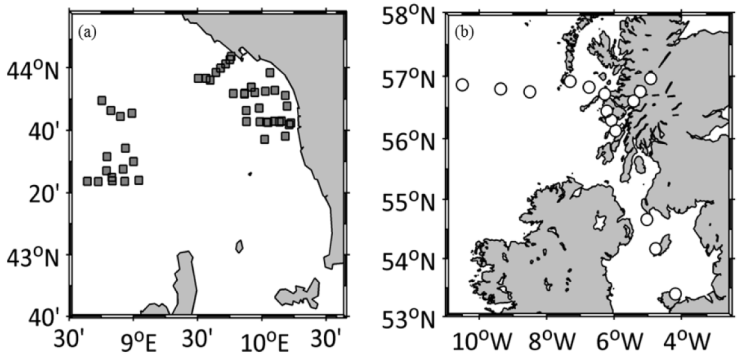


Fig. 1. Station maps for (a) Ligurian Sea (LS), March 2009, and (b) West Coast of Scotland (WCS), June 2012.

### *2.2 IOP measurements*

For both cruises, *in situ* profiles of $a(\lambda)$ and $c(\lambda)$ were collected with a 25 cm pathlength AC-9 (WetLabs Inc.). Absorption and attenuation coefficients were determined for 9 different wavebands (10 nm FWHM) centred on 412, 440, 488, 510, 532, 555, 650, 676 and 715 nm. The AC-9 was calibrated before and during each cruise with ultrapure water (Milli-Q, Millipore) and data were corrected for the temperature and salinity dependence of pure seawater [40] and for scattering errors using three different correction methods: (1) the *proportional* correction [18], (2) the *semi-empirical* correction [25] and (3) the *iterative* method [17].

The *proportional* correction method assumes negligible NIR absorption and a wavelength independent scattering phase function. Absorption measurements were corrected using

#264909 Received 11 May 2016; accepted 28 May 2016; published 15 Jun 2016

accompanying attenuation measurements to estimate a wavelength dependent scattering error using

$$a_{ac9}(\lambda) = a_m(\lambda) - a_m(715)\frac{c_m(\lambda) - a_m(\lambda)}{c_m(715) - a_m(715)} \quad (1)$$

where $a_{ac9}$ is the corrected non-water absorption at a given wavelength, $\lambda$, the subscript $m$ denotes uncorrected measured signals and 715 nm is used as the reference NIR wavelength. The assumptions underpinning this correction might not hold for waters with high levels of non-biogenic minerals or CDOM which can lead to increased NIR absorption [41]. Additionally, the extent to which the scattering phase function can be considered wavelength dependent or otherwise remains a subject of debate, with highly turbid coastal areas the most likely area for the occurrence of significant wavelength dependence [42,43].

The *semi-empirical* correction [25] follows the same basic form as the proportional correction but introduces two new terms that provide for non-zero NIR absorption values and basic correction of the scattering error for attenuation measurements. In this case data are corrected using

$$a_{ac9}(\lambda) = a_m(\lambda) - \left[a_m(715) - a_{emp}(715)\right]\frac{(1/e_c)c_m(\lambda) - a_m(\lambda)}{(1/e_c)c_m(715) - a_{emp}(715)} \quad (2)$$

where $1/e_c$ is a scattering correction for the attenuation measurement and $a_{emp(715)}$ is an empirical estimate of the NIR absorption coefficient. Boss *et al.* [23] found an average value of $e_c = 0.56$ for a single wavelength. This attenuation correction is used in Eq. (2) and for subsequent use of attenuation data in RT simulations testing the performance of the *semi-empirical* correction method. $a_{emp}(715)$ is an empirical estimation of NIR absorption and is given by

$$a_{emp}(715) = 0.212\left[a_m(715)\right]^{1.135} \quad (3)$$

The *iterative* correction [17] is based on prior Monte Carlo simulations of both the absorption and attenuation flow cells. Scattering errors for both the absorption and attenuation sensors are phase function dependent, and additional backscattering data are required to give particulate backscattering ratios that are used in the model to predict appropriate error values. In addition, the error model has to be tuned on an instrument-specific basis for the effect of imperfect wall reflectance in the absorption tube. This was done for the AC-9 instrument used in this study using associated PSICAM data to select an appropriate wall reflectance value for this sensor [17]. This correction method makes no assumptions about NIR absorption and is designed to accommodate wavelength dependent scattering phase functions, should they occur.

A WETLabs BB-9 was mounted alongside the AC-9 to make concurrent depth profile measurements of backscattering. Backscattering coefficients were calculated based on measurements of the VSF at an effective scattering angle of 117°, for nine wavebands at 412, 440, 488, 510, 532, 595, 650, 676 and 715 nm. Backscattering data were subsequently interpolated to AC-9 wavelengths and measurements were corrected according to the BB-9 manual [44]: correction for pathlength absorption was performed using AC-9 absorption data corrected with the *proportional* method; the total VSF was converted to particulate VSF by subtraction of water VSF calculated from [45]; $\beta_p(117°,\lambda)$ was converted to particulate backscattering coefficient, $b_{bp}(\lambda)$. A $\chi$-factor of 1.1, as suggested by Boss and Pegau [46], was used to derive $b_{bp}$ from $\beta_p$ for data collected in the LS. This approach was revised for processing of the WCS data following changes in the manufacturer's calibration process and $\chi = 0.9$ was used for this data set in accordance with Sullivan *et al.* [47]. Whilst no dark signals were measured on board, particulate backscattering coefficients were always > 0.001 $m^{-1}$ and the effect of drifting dark signals can be considered negligible [48].

#264909 Received 11 May 2016; accepted 28 May 2016; published 15 Jun 2016

*2.3 Radiometric measurements*

Two radiometer configurations were used to compile the data set used here. LS radiometric data were collected using a free-falling HyperPro profiler (Satlantic Inc.) configured with hyperspectral downwards irradiance, $E_d(z,\lambda)$, and upwards radiance, $L_u(z,\lambda)$ sensors. The profiling radiometer was deployed in a multicast mode to sample the surface layer multiple times at each station to calculate the mean light field accurately in the top 10 m. In addition, where possible, a deep cast was collected to study light penetration below the surface layer. The median of all casts was calculated for 1 m binned profiles (further information below). WCS radiometric data were measured with TriOS RAMSES hyperspectral radiometers giving upwards radiance, $L_u(\lambda,z)$, upwards irradiance, $E_u(\lambda,z)$, and downwards irradiance, $E_d(\lambda,z)$. This profiling package was lowered to specific depths and data accumulated over a two minute period at each depth. In this case, the final radiometry profile was composed of median values of each radiometric parameter at each depth step. A spectral stray-light correction (SLC) was applied to all radiometric data collected with the HyperPro (LS cruise) following the suggestions of the NASA Carbon Cycle & Ecosystem Joint Science Workshop [49]. The SLC in a spectroradiometer can be described by the instrument's spectral line spread function (SLSF). SLC was performed at the NIST Spectral Irradiance and Radiance Responsivity Calibrations using Uniform Sources (SIRCUS) by characterizing the scattering properties of spectrographs and imaging systems using five continuously tunable lasers (400 to 800 nm) to reduce the magnitude of errors arising from spectral and spatial stray light by one to two orders of magnitude. This additional correction leads to slightly lower $E_d$ and $L_u$ values compared to the uncorrected HyperPro data, especially at wavelengths in the blue.

On both cruises, measurement artefacts in radiometric profile data were reduced following NASA Ocean Optics protocols [50]: the ship was positioned so that ship shadow effects were minimised and a deck reference sensor was mounted on the ship's superstructure measuring downwelling above surface irradiance, $E_s(t,\lambda)$. All underwater radiometry profiles were corrected for changes in the incident solar radiation during a cast sequence by normalising to coincident surface irradiance data, $E_s(t,\lambda)$, and then rescaling to the median surface irradiance, $\langle E_s(t,\lambda)\rangle$, calculated over the duration of the *in situ* profiles using

$$\hat{I}_x(z,\lambda) = \frac{I_x(z,\lambda)\langle E_s(t,\lambda)\rangle}{E_s(t,\lambda)} \tag{4}$$

where $I_x$ represents any of $E_d$, $L_u$ or $E_u$. Multicast profiles were merged into a single profile before final processing broadly following Sanjuan Calzado *et al.* [51]. All radiometric profile data were filtered to remove high tilt values and outliers beyond 95% prediction intervals associated with wave focusing effects were also removed.

The TriOS sensors used on the WCS cruise were re-calibrated post-cruise during which process damage to the $E_s$ sensor was discovered. Post-cruise re-calibration of the $E_s$ sensor produced above surface $E_s$ data that was subsequently found to be inconsistent with below surface $E_d$ data, tested by RT modelling. Therefore, it was necessary to adopt an alternative strategy to derive above surface $E_s$ data for input to RT models for the WCS data set. This involved extrapolating $E_d(555, z)$ up to and through the sea surface and using this value to rescale measured $E_s$ spectra using:

$$E_{s,ext}(\lambda) = \frac{E_s(\lambda)E_{s,ext}(555)}{E_s(555)} \tag{5}$$

where $E_{s,ext}$ values are new extrapolated spectral sky irradiances, and $E_s$ values are the original measured solar downwards sky irradiances derived from extrapolation of $E_d(555,z)$. The performance of this approach was assessed by comparing measured and modelled $E_d$ data at the shallowest depth available. Figure 2 demonstrates that this approach provides input $E_s$ data that are consistent with subsurface $E_d$ data across the full spectral range considered here

#264909 Received 11 May 2016; accepted 28 May 2016; published 15 Jun 2016

(RMS%E = 9.9%). Although this approach effectively limits one degree of freedom, analysis of optical closure for $E_d$ at depth and for $L_u$ and other associated products remains valid.

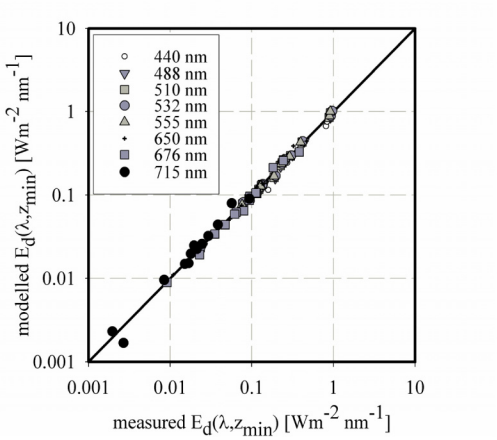


Fig. 2. Comparison of modelled and measured subsurface $E_d$ values for all WCS stations as test of method to derive $E_s$ by extrapolation. Input AC-9 data has been corrected using the *proportional* correction.

### *2.4 Radiative transfer modelling*

Underwater light fields were modelled using EcoLight 5.0 (Sequoia Scientific). This version of the RT model was chosen in preference to the more complete Hydrolight version in respect of the potential application for incorporating RT models directly into coupled physical-ecosystem models, for which EcoLight is better suited. Comparison with a complete Hydrolight run for one station did not show any significant deviation for the parameters of interest here. The model was provided with *in situ* profiles of absorption, attenuation and backscattering data processed using the three scattering correction approaches discussed above. EcoLight generates Fournier-Forand scattering phase functions from derived particulate backscattering ratios [30,52]. The median above surface irradiance spectrum, $\langle E_s(t,\lambda)\rangle$, and an estimate of percentage cloud cover, were used to parameterise incoming solar radiation. Modelling of inelastic scattering was restricted to Raman scattering by water. Fluorescence by CDOM and phytoplankton were not included in simulations as this would require estimation of constituent concentration profiles and quantum yields. This goes beyond the scope of this paper which is deliberately restricted to assessing optical closure performance considering the quality of IOP inputs. Output wavelengths and depths were chosen to match *in situ* IOP and radiometry measurements to avoid artefacts due to inter- or extrapolation of the data.

### *2.5 Optical closure assessment*

The degree of optical closure was tested for a range of radiometry and AOP parameters including: $E_d(z)$ and $L_u(z)$ at 440 nm, 532 nm and 650 nm (the analysis does not extend to longer wavelengths to avoid obvious artefacts associated with chlorophyll fluorescence; 412 nm was excluded from analysis for the WCS data set as the backscattering sensor failed at this wavelength), *PAR* as a function of depth, and the spectral radiance reflectance, $R_L(\lambda)$, at $z_{min}$, the closest measurement to the sea surface. Each of the parameters varied over orders of magnitude with depth for these data sets, so data were log-transformed before regressions were applied to find best-fit slopes for each profile. The range and median of these slopes are used as primary measures of the degree to which optical closure has been achieved. Slopes greater than one indicate modelled values decreasing too rapidly with depth and vice versa.

#264909 Received 11 May 2016; accepted 28 May 2016; published 15 Jun 2016

Additionally, root mean square percentage errors, RMS%E, (Eq. (6)) provide information on the spread between modelled and measured data sets.

$$RMS\%E = \sqrt{\frac{1}{n}\sum_{1}^{n}\left(\frac{x_{model} - x_{meas}}{x_{meas}} \times 100\right)^2} \quad (6)$$

## 3. Results

### *3.1 Comparison of AC-9 scattering correction methods*

The impact of the three different AC-9 correction approaches on absorption and attenuation data is presented for two example WCS stations. ST05 (56° 43.317' N, 6° 16.585' W) is a relatively clear station and ST12 (56° 45.503' N, 5° 13.544' W) is a more turbid station. Figures 3(a) and 3(b) show only limited differences between scatter corrections on absorption data for these stations (maximum 0.017 $m^{-1}$ across the spectrum). The *proportional* correction results in slightly lower absorption coefficients in the red due to the assumption of zero absorption at 715 nm, but the effect is minimal, particularly considering the strength of water absorption at these wavelengths (not included in these plots). Larger deviations are observed between the different corrections for attenuation spectra (Figs. 3(c) and 3(d)).

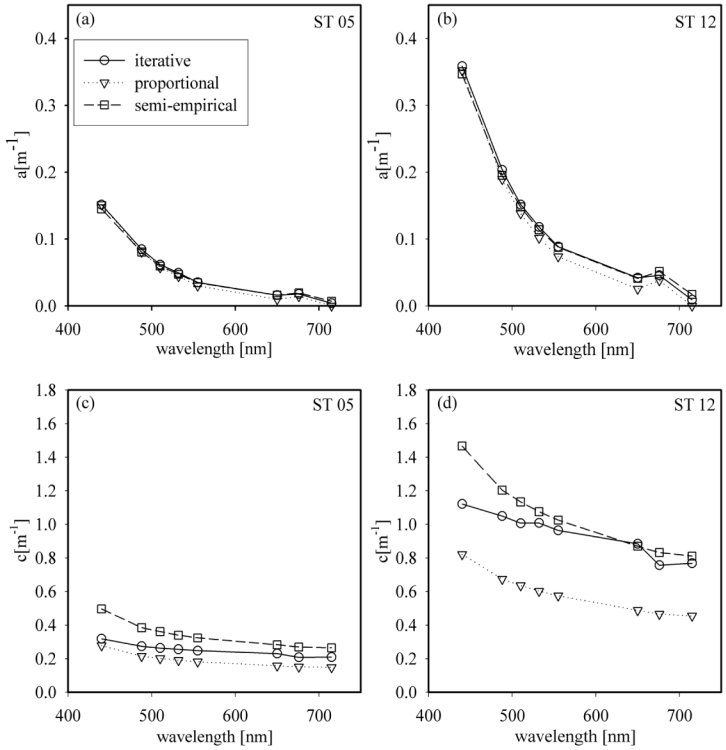


Fig. 3. AC-9 absorption (a) and (b) and attenuation (c) and (d) spectra measured at two stations from the WCS cruise, showing the effects of three different AC-9 corrections: *proportional*, *iterative* and *semi-empirical*.

The *proportional* correction does not include an attenuation correction whereas the *semi-empirical* increases the attenuation by a constant factor of 1.78. The *iterative* correction increases attenuation by varying amounts (spectrally and from station to station) – resulting in either higher or lower beam attenuation coefficients compared to the *semi-empirical* correction, but always higher than the uncorrected data. It should be noted that the *iterative*

#264909 Received 11 May 2016; accepted 28 May 2016; published 15 Jun 2016

correction returned negative absorption coefficients for wavelengths ≥650 nm for two WCS stations which sampled a strongly backscattering coccolithophore bloom. These two stations were found to be anomalous in several ways (see later for further discussion).

Modelled $E_d(650)$ profiles for ST05 and ST12 showed little sensitivity to AC-9 correction methods despite the large differences in corrected beam attenuation (Figs. 4(a) and 4(b)). Modelled $L_u(650)$ profiles were similarly insensitive to the choice of scattering correction, with ST12 perhaps showing a little more variation between the *proportional* versus the other two scattering corrections (Figs. 4(c) and 4(d)). These results are in agreement with Gordon [53] who found that forward scattered light does not have a significant effect on RT model outputs. In what follows, the *proportional* correction is used for all modelled data presented graphically because it is the easiest to implement and most commonly applied in literature. The impact of alternative scattering corrections on optical closure is demonstrated in tabulated data only.

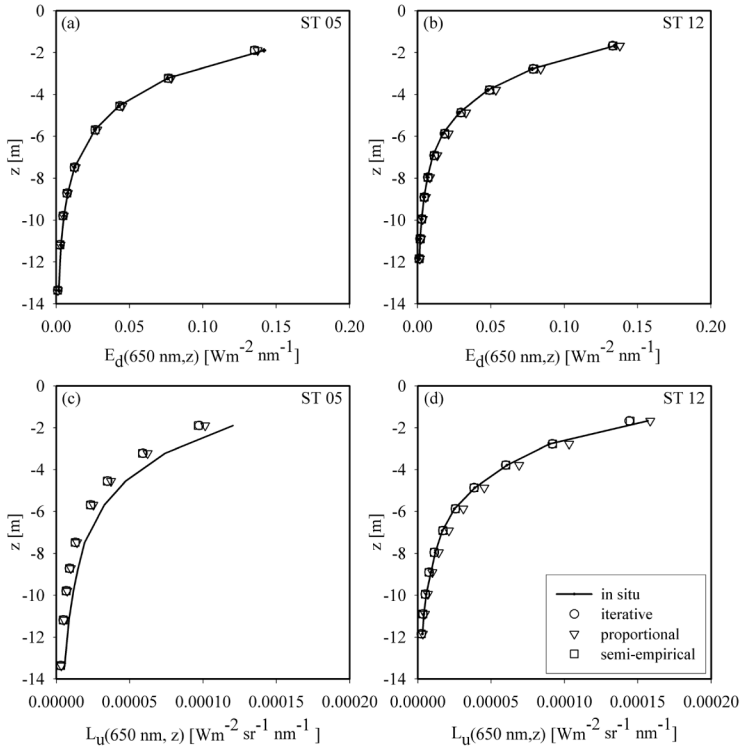


Fig. 4. Modelled and measured $E_d$ (a) and (b) and $L_u$ (c) and (d) profiles measured at two stations, ST05 (clear water) and ST12 (sea loch water), from the WCS cruise. The RT model was populated with AC-9 data corrected with three different corrections: *proportional, iterative* and *semi-empirical*.

### *3.2 $E_d$ and PAR closure*

Agreement between modelled and measured $E_d$ was between 12% - 38% RMS%E for both cruises across all three wavebands examined, 440 nm, 532 nm and 650 nm (Fig. 5). Closure improved with increasing wavelength for both data sets, with median best-fit slopes closest to 1.0 at 650 nm (Tables 2 and 3). The lowest overall spread in data, however, was observed at 532

#264909 Received 11 May 2016; accepted 28 May 2016; published 15 Jun 2016

**Table 2. Minimum, maximum and median slopes obtained from linear regressions of modelled vs. measured depth profiles over all stations of the LS cruise in 2009, for each of the AC-9 scattering corrections. Slope values greater than one represent a tendency of modelled data to underestimate *in situ* value.**

| | proportional | | | iterative | | | semi-empirical | | |
|---|---|---|---|---|---|---|---|---|---|
| LS | median | min | max | median | min | max | median | min | max |
| $E_d$(440 nm) | 1.14 | 0.80 | 1.70 | 1.16 | 0.83 | 1.71 | 0.97 | 0.72 | 1.43 |
| $E_d$(532 nm) | 1.11 | 0.83 | 1.64 | 1.14 | 0.90 | 1.68 | 0.99 | 0.60 | 1.47 |
| $E_d$(650 nm) | 1.07 | 0.96 | 1.22 | 1.07 | 0.96 | 1.26 | 1.03 | 0.93 | 1.22 |
| $L_u$(440 nm) | 1.09 | 0.62 | 1.28 | 1.14 | 0.63 | 1.47 | 0.92 | 0.60 | 1.31 |
| $L_u$(532 nm) | 1.06 | 0.48 | 1.23 | 1.13 | 0.48 | 1.47 | 0.94 | 0.47 | 1.53 |
| $L_u$(650 nm) | 1.14 | 0.89 | 1.83 | 1.17 | 0.91 | 1.92 | 1.09 | 0.85 | 1.75 |
| PAR(z) | 0.96 | 0.64 | 1.26 | 1.07 | 0.88 | 1.40 | 1.05 | 0.84 | 1.39 |

**Table 3. Minimum, maximum and median slopes obtained from linear regressions of modelled vs. measured depth profiles over all stations of the WCS cruise in 2012, for each of the AC-9 scattering corrections. Slope values greater than one represent a tendency of modelled data to underestimate *in situ* value.**

| | proportional | | | iterative | | | semi-empirical | | |
|---|---|---|---|---|---|---|---|---|---|
| WCS | median | min | max | median | min | max | median | min | max |
| $E_d$(440 nm) | 1.22 | 1.06 | 1.43 | 1.21 | 1.08 | 1.36 | 1.24 | 1.07 | 1.60 |
| $E_d$(532 nm) | 1.03 | 0.90 | 1.36 | 1.09 | 0.96 | 1.42 | 1.14 | 0.96 | 1.46 |
| $E_d$(650 nm) | 1.01 | 0.94 | 1.29 | 1.04 | 0.96 | 1.29 | 1.05 | 0.97 | 1.40 |
| $L_u$(440 nm) | 1.19 | 1.04 | 1.35 | 1.19 | 1.03 | 1.35 | 1.19 | 1.03 | 1.50 |
| $L_u$(532 nm) | 1.07 | 0.91 | 1.40 | 1.16 | 0.94 | 1.58 | 1.19 | 0.94 | 1.52 |
| $L_u$(650 nm) | 1.11 | 0.95 | 1.42 | 1.15 | 0.97 | 1.38 | 1.14 | 0.97 | 1.57 |
| PAR(z) | 1.06 | 0.92 | 1.28 | 1.09 | 0.99 | 1.31 | 1.13 | 1.00 | 1.42 |

**Table 4. RMS%E for modelled data for LS and WCS cruises. Comparison between different AC-9 scattering corrections.**

| | proportional | | iterative | | semi-empirical | |
|---|---|---|---|---|---|---|
| RMS%E | LS | WCS | LS | WCS | LS | WCS |
| $E_d$(440 nm) | 22.3 | 33.9 | 22.8 | 30.7 | 20.0 | 37.9 |
| $E_d$(532 nm) | 15.3 | 12.3 | 18.0 | 13.0 | 19.7 | 21.4 |
| $E_d$(650 nm) | 26.1 | 22.6 | 28.4 | 22.4 | 22.9 | 25.5 |
| $L_u$(440 nm) | 30.4 | 46.1 | 33.0 | 41.3 | 36.7 | 49.0 |
| $L_u$(532 nm) | 18.9 | 33.8 | 25.6 | 37.4 | 62.9 | 45.6 |
| $L_u$(650 nm) | 35.9 | 32.8 | 40.4 | 35.0 | 30.8 | 40.1 |
| PAR(z) | 21.0 | 15.1 | 18.1 | 14.9 | 15.8 | 24.4 |
| $R_L(\lambda,z_{min})$ | 24.0 | 32.6 | 24.8 | 32.2 | 30.2 | 31.4 |

nm with an RMS%E < 16% for the proportional correction (Table 4). The degree of optical closure was slightly weaker in the blue waveband for WCS stations. Superior closure for blue waveband data for the LS data set might be due to the additional straylight correction applied to radiometric data collected on the LS cruise. The degree of optical closure obtained for the two coccolithophore stations in the WCS data set was weaker still. Together with the poor performance of the *iterative* AC-9 correction at these coccolithophore stations, this potentially

#264909 Received 11 May 2016; accepted 28 May 2016; published 15 Jun 2016

points towards problems with the angular distribution of the modelled scattering phase function for this special case. Median best fit slopes for *PAR* (Fig. 6) varyied from unity by less than 10% for all scattering corrections, with this level of success at least partly due to the low sensitivity of *PAR* to wavelength dependent artefacts. The RMS%E for *PAR* was <21% when using the *proportional* correction for the LS cruise and about 15% for the WCS cruise (Table 4).

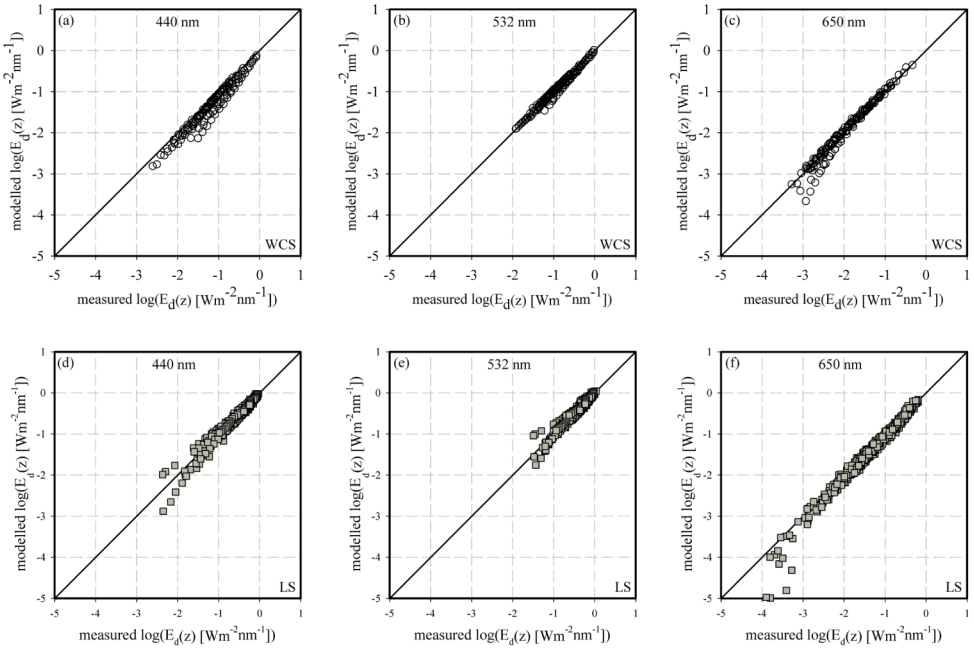


Fig. 5. Agreement between modelled and measured $E_d(\lambda,z)$ for data collected off the West Coast of Scotland (WCS – (a), (b) and (c)) and in the Ligurian Sea (LS – (d), (e) and (f)). Results are presented for three different wavelengths, 440 nm, 532 nm and 650 nm (from left to right). All IOP measurements used as input for the RT modelling were corrected using the *proportional* correction.

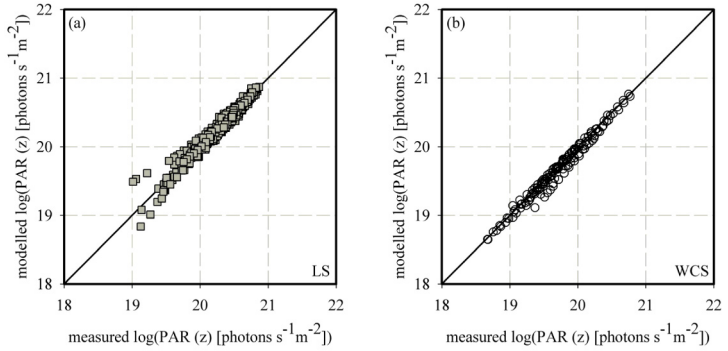


Fig. 6. Correlation of modelled and measured data for *PAR(z)* for (a) the Ligurian Sea (LS) and (b) a data set measured off the West Coast of Scotland (WCS).

### *3.3 $L_u$ and $R_L$ closure*

Optical closure performance for $L_u$ was between 18 – 63% RMS%E (Fig. 7) and again improved with increasing wavelength with median best-fit slopes closest to unity at 650 nm (Tables 2 and 3).The apparent increase in RMS%E for $L_u$ compared to $E_d$ data potentially

#264909 Received 11 May 2016; accepted 28 May 2016; published 15 Jun 2016

reflects differences in signal to noise ratio for the *in situ* measured radiometry. Overall there is very little observable impact on model performance from choice of scattering correction. Median best-fit slopes are generally greater than unity indicating a general tendency for modelled $L_u$ values to underestimate *in situ* measurements. However, underestimation of modelled $L_u$ is largely compensated by corresponding underestimates of $E_d$, resulting in modelled subsurface $R_L$ data that is generally in quite good agreement with measurements (Fig. 8), with both data sets showing modest underestimates for modelled values across the spectral range. Some of this underestimation may be due to non-inclusion of fluorescence emission effects which tends to impact on $L_u$ (and therefore $R_L$) more than $E_d$. Certainly extension of the analysis to 676 nm where chlorophyll fluorescence effects are much greater results in significantly greater underestimation of both $L_u$ and $R_L$ (data not shown).

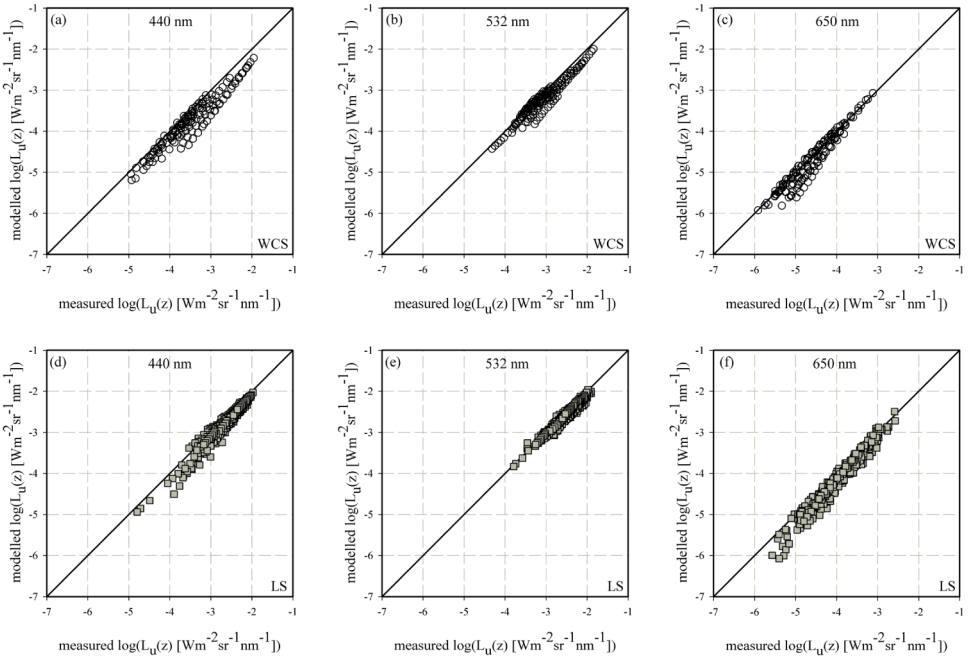


Fig. 7. Agreement between modelled and measured $L_u(\lambda,z)$ for data collected off the West Coast of Scotland (WCS – (a), (b) and (c)) and in the Ligurian Sea (LS – (d), (e) and (f)). Results are presented for three different wavelengths, 440 nm, 532 nm and 650 nm (from left to right). All IOP measurements used as input for the RT modelling were corrected using the *proportional* correction.

It is important to note that the model tendency to underestimate $E_d$ and $L_u$ with depth occurs for both data sets. This suggests there is at least one, and maybe more than one, outstanding systematic error in the closure scheme. The use of two nominally independent radiometer systems could be used to justify eliminating radiometer errors as a consideration. However, it remains possible that both could be subject to a shared limiting characteristic. For example, both radiometer systems might have imperfections in cosine collector performance that might generate systematic errors with changing light field structure at depth. As mentioned previously, there is also the question of unresolved or poorly parameterized angular structure in the volume scattering function which has the potential to affect both IOP generation and RT model performance. Of these two options, and taking into account all of the available observations, it seems more likely that unresolved angular scattering characteristics are the problem here, but neither possibility can be ruled out with certainty.

#264909 Received 11 May 2016; accepted 28 May 2016; published 15 Jun 2016

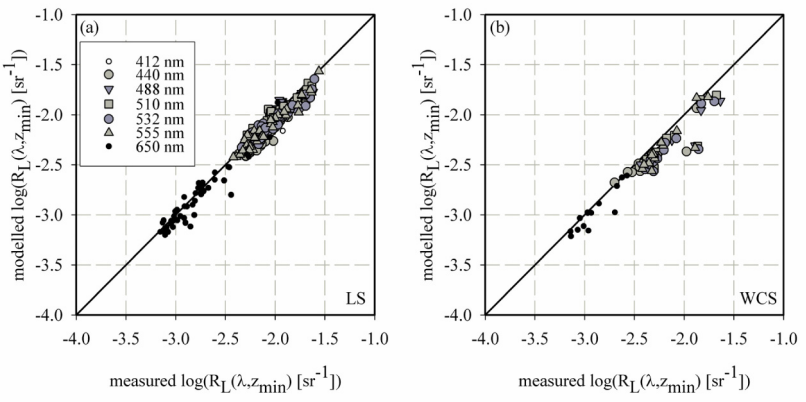


Fig. 8. Agreement between modelled and *in situ* data for radiance reflectance, $R_L(\lambda)$ just beneath the surface for two data sets collected in the Ligurian Sea (a) and off the West Coast of Scotland (b). 412 nm was excluded from the analysis for the WCS data set.

## 4. Discussion

### *4.1 Impact of AC-9 scattering corrections on optical closure*

The recent development of new scattering corrections for AC-9 absorption and attenuation data was a key motivation for this reassessment of our ability to achieve optical closure. In the end, the vast majority of stations in our data set showed little sensitivity to the choice of AC-9 scattering correction method. Reasons for this include: (a) the data set only included a small number of highly turbid stations where the effect of new corrections are expected to be most significant, (b) the greatest effect of scattering corrections on AC-9 data is for attenuation (and therefore scattering) values which have little impact on optical closure [53], and (c) such absorption differences as were observed occurred in the red-NIR which is dominated by water absorption for optical closure purposes. For this data set, except for a few special cases, the *proportional* scattering correction method provided results at least as good as more complicated scattering corrections. Fundamental problems remain for the stations in strongly scattering waters sampled during the WCS cruise, and are likely to apply to similarly turbid phytoplankton bloom or mineral particle resuspension events elsewhere. More work is required to establish a robust picture in these scenarios, but there is circumstantial evidence from this data set that points to limitations in the parameterisation of the VSF being a contributing feature to difficulties in successfully correcting AC-9 data using the *iterative* correction method and in achieving optical closure in these waters.

### *4.2 Optical closure in moderately turbid waters*

The degree of closure achieved in the two sample areas was broadly comparable, with a general tendency to overestimate the attenuation of both $E_d$ and $L_u$ with depth (median best-fit slopes >1). The median best-fit slopes (0.92 – 1.24) gives one measure of 'typical' closure performance for depth profiling radiometry. Of course, the much wider maximum and minimum ranges of these slopes serve as a warning that closure performance might be significantly less satisfactory for individual stations. Generally strong performance for *PAR* closure (RMS%E <25%) is particularly welcome for ecosystem modelling applications. Surface reflectance results were only slightly less satisfactory (RMS%E < 33%) but this is potentially a more significant error for OCRS closure applications.

### *4.3 Model parameterisation*

The selection of AC-9 scattering correction has been found to only weakly influence optical closure performance for this data set. RMS%E for closure with different scattering

#264909 Received 11 May 2016; accepted 28 May 2016; published 15 Jun 2016

corrections typically varied by less than 10% and in the worst case reached a maximum variation of 44%. Further uncertainty lies in the parameterisation of the VSF and in potentially limiting assumptions supporting $b_b$ measurements. The backscattering coefficient is derived by a simple extrapolation of a single measure of the VSF through use of a so-called $\chi$ factor. A single value of the $\chi$ factor is used for all data leading to two possible error scenarios if we assume the radiometry data are robust at all depths: (a) the value of the $\chi$ factor is incorrect and a corrected value would give better general closure, or (b) selection of a single $\chi$ factor potentially masks variability associated with differences in the angular distribution of scattering for stations with different constituent compositions. Varying the $\chi$ factor by up to a factor of 2 was found to partially improve closure with $L_u$ data but at the expense of deteriorating closure with $E_d$. This leads to the conclusion that any error in $b_b$ would have to be more complex than a simple error in the choice of a single value of the $\chi$ factor. Poor performance in the coccolithophore bloom and highly turbid waters for both the *iterative* AC-9 correction and for optical closure potentially points to unresolved issues in the parameterisation of the VSF that might continue to affect $b_b$, AC-9 and RT modelling processes. This conclusion is consistent with results of a recent study [54] that illustrated potential limitations in the parameterization of theoretical scattering phase functions for algal cultures and mineral suspensions. Angularly resolved spectral VSF data is urgently required for these waters.

This study restricted modelling of inelastic scattering effects to the ubiquitous Raman scattering by water. Not including chlorophyll or CDOM fluorescence is a potential source for underestimation of $E_d$ and $L_u$ at wavebands in the green and red / NIR. Tzortziou *et al.* [31] showed that including chlorophyll fluorescence improved optical closure from 30 to 40% underestimation to 4-8%, and including CDOM fluorescence improved agreement by 2-5%, at respective fluorescence emission wavelengths. Using RT simulations, the effect of including fluorescence for these data sets was tested using very broad brush estimates for key variables (concentrations and quantum yields) and results showed that whilst $L_u$ closure could be improved, there was no significant impact on $E_d$. It is therefore unlikely that inclusion of inelastic effects would be sufficient, on its own, to address the residual closure discrepancies observed here. Chlorophyll and CDOM fluorescence yields are known to be highly variable and considerable selective tuning is possible which would detract from the rigorous approach that has been attempted here.

## 5. Conclusion

Radiative transfer modelling has been used to assess the degree of optical closure that can be achieved for a range of clear to moderately turbid waters using *in situ* IOP measurements. The depth range considered extends to the maximum depth for which *in situ* radiometry data was collected, typically surface waters down to an average of 12 m, but in some cases as deep as 35 m, greatly exceeding the range previously considered [31]. It has been shown that there is an overall tendency for simulations to slightly underestimate both $E_d$ and $L_u$ throughout the water column by factors that vary with parameter, wavelength and IOP correction method. Discrepancies between measured and modelled radiometry data invariably accumulate with increasing depth. This, together with the exponential decrease in signal with depth, poses a problem for generating meaningful error estimates. Using median regression slopes between measured and modelled log-transformed radiometry data to characterize the degree of closure, this tendency to underestimate both $E_d$ and $L_u$ is expressed as slope values that are typically within ~15% of unity. However, there are instances where the mis-match between modelled and measured radiometry is significantly greater, with best-fit slopes in some cases almost reaching a factor of 2. The source of these residual errors remains unknown, but does not appear to be associated with scattering correction errors for *in situ* absorption and attenuation data. A combination of inelastic scattering effects, unresolved angular structure in the volume scattering function and radiometer instrument angular response errors are suggested as potential contributors.

#264909 Received 11 May 2016; accepted 28 May 2016; published 15 Jun 2016

A key driver for this study is the provision of key variables such as *PAR* and surface remote sensing reflectance, with associated uncertainties, for use in subsequent modelling activities. *PAR* is typically modelled to within 15-25% of measured values, while subsurface remote sensing reflectance is modelled to within 24-33%. These results provide a best-case scenario when full profiles of IOPs are available (with the exception of angularly resolved spectral VSF). Optical closure applications relying on less complete data sets may be expected to achieve less satisfactory closure and user expectations / mission requirements should be managed accordingly.

**Acknowledgments**

The authors would like to thank the skippers and crews of *NR/V Alliance* (BP'09 cruise) and *R/V Prince Madog* for their help and support in assembling these data sets. This work was supported by NERC Advanced Fellowship NE/E013678/1 to McKee, NERC Standard Grant NE/H022090/1 to Bowers, Nimmo-Smith and McKee and CMRE NATO contract, Scientific Program of Work 2009 to C. Trees, British Council Travel Grant to Bengil.